Fluoride ion diffusion of superionic $PbSnF_4$ studied by nuclear magnetic resonance and impedance spectroscopy

2002 J. Phys.: Condens. Matter 14 7233

(http://iopscience.iop.org/0953-8984/14/30/312)

INSTITUTE OF PHYSICS PUBLISHING JOURNAL OF PHYSICS: CONDENSED MATTER

J. Phys.: Condens. Matter **14** (2002) 7233–7244 PII: S0953-8984(02)33403-9

Fluoride ion diffusion of superionic $PbSnF_4$ studied by nuclear magnetic resonance and impedance spectroscopy

Mohamad M Ahmad[1], **Koji Yamada and Tsutomu Okuda**

Department of Chemistry, Graduate School of Science, Hiroshima University, Higashi-Hiroshima 739-8526, Japan

Received 4 February 2002, in final form 26 June 2002
Published 17 July 2002
Online at stacks.iop.org/JPhysCM/14/7233

Abstract

Superionic material $PbSnF_4$ prepared by precipitation from aqueous solution was characterized by x-ray diffraction, DTA and ^{19}F nuclear magnetic resonance (NMR) techniques. The temperature and frequency dependence of the conductivity, the modulus and the dielectric properties were investigated by means of impedance spectroscopy. The Arrhenius plot of the dc conductivity shows a gradual slope change around 355 K from a high-activation-energy ($E_\sigma = 30$ kJ mol^{-1}) region to a low-activation-energy region ($E_\sigma = 22$ kJ mol^{-1}). At lower temperatures the real part of the ac conductivity exhibited a power-law behaviour as found in most ionic conductors. At high temperatures, on the other hand, a low-frequency dispersion of the conductivity was observed due to the space charge polarization, which resulted from the high ionic conductivity. An extremely large dielectric constant was observed with decreasing frequency due to the space charge polarization. A dielectric anomaly was also observed around the phase transition temperature. The modulus formalism was used to estimate the conductivity relaxation times and was compared with those from the line width transition of the ^{19}F NMR.

1. Introduction

Superionic $PbSnF_4$ is the highest-performance fluoride ion conductor. Its conductivity reaches 10^{-3} S cm^{-1} at room temperature, which is the highest value among well known anionic conductors [1]. $PbSnF_4$ was first synthesized by Donaldson *et al* [2] either by precipitation from aqueous solution or by high-temperature reaction between SnF_2 and PbF_2. There are several different phases of $PbSnF_4$ depending on the method of preparation. α-$PbSnF_4$ (monoclinic) can be obtained either by a precipitation from aqueous solution or by a direct solid-state reaction of a 1:1 mixture of SnF_2 and PbF_2 at 250 °C, whereas orthorhombic $PbSnF_4$ was obtained from

[1] On leave from: Department of Physics, Faculty of Education, Assiut University, El-Kharga, The New Valley, Egypt.

0953-8984/02/307233+12$30.00

aqueous solution with the addition of HF to SnF_2 solution. In addition, tetragonal β-$PbSnF_4$ was prepared through the solid-state reaction route at 400 °C and γ-$PbSnF_4$ phase was obtained by ball milling α, β or orthorhombic $PbSnF_4$ [3].

Several authors have reported phase transitions in $PbSnF_4$. While Reau *et al* [1] and Chadwick *et al* [4] showed a transition from a monoclinic (α) to a tetragonal (β) phase, which caused a break in the conductivity–temperature curve around 353 K, Kanno *et al* [5] found no symmetry change at this temperature and attributed this break in the conductivity curve to a diffuse phase transition. The high fluoride ion mobility has been studied by the complex impedance method on polycrystalline samples of $PbSnF_4$ [1, 5, 6]. This exceptionally high fluoride ion conductivity of $PbSnF_4$ has been used recently for the fabrication of a fast-response amperometric oxygen sensor at room temperature [7, 8]. In the present work, $PbSnF_4$ was synthesized by precipitation from aqueous solution and characterized by x-ray powder diffraction, differential thermal analysis and ^{19}F NMR. In order to understand the electric properties of this material, the data from the complex impedance measurements of the superionic $PbSnF_4$ were analysed by means of various formalisms, such as complex conductivity, $\sigma^* = \sigma' + j\sigma'' = 1/Z^*$, electric modulus, $M^* = j\omega C_0 Z^* = 1/\varepsilon^*$, and complex permittivity, $\varepsilon^* = \varepsilon' - j\varepsilon''$, which was related to σ^* by the Maxwell relation,

$$\sigma^* = j\omega\varepsilon_0\varepsilon^*, \tag{1}$$

where ω is the angular frequency, C_0 is the capacitance of the empty cell and ε_0 is the permittivity of free space. The modulus treatment was proved to be a useful formalism because the conductivity relaxation times were easily estimated without suffering from the interfacial effects.

2. Experimental details

$PbSnF_4$ was obtained by stirring solid α-PbF_2 in a fresh aqueous solution of SnF_2 at room temperature with a Pb/Sn ratio $\leqslant$0.5 for 10 h. The white precipitate of $PbSnF_4$ was then filtered off immediately, washed with distilled water and dried at about 100 °C for 1 h. The sample was annealed at about 150 °C for 10 h. The reaction product was characterized by x-ray powder diffraction using a Rigaku Rint PC system with graphite-monochromatized Cu Kα radiation (λ = 1.5405 Å). DTA measurement was performed using a sealed tube in the temperature range from 300 to 500 K at a heating rate of 4 K min^{-1}.

For impedance measurements, the fine powder of the polycrystalline $PbSnF_4$ was compressed under a pressure of 4 tons cm^{-2} to obtain a pellet of 13 mm diameter and 2 mm thickness. Complex impedance measurements were performed by the two-terminal method. Carbon paint was evenly applied on both sides of the pellet for better electrical contact; the sample was then held between two spring-loaded electrodes. The impedance $|Z^*|$ and phase angle θ were measured with a computer-interfaced HIOKI 3532 *LCR* meter (42 Hz–5 MHz) in the temperature range from 150 to 478 K with a heating rate of 2 K min^{-1}.

^{19}F NMR spectra were observed using a homemade pulsed spectrometer at 6.4 T with a corresponding Larmor frequency of 255.2 MHz. The dead time of our spectrometer after an rf pulse was typically 4–5 μs.

3. Results and discussion

3.1. Sample characterization by means of DTA and x-ray diffraction

The DTA measurement of $PbSnF_4$ showed an endothermic peak at 340 K on heating, while a less intense exothermic peak at 335 K on cooling was observed. These temperatures are in

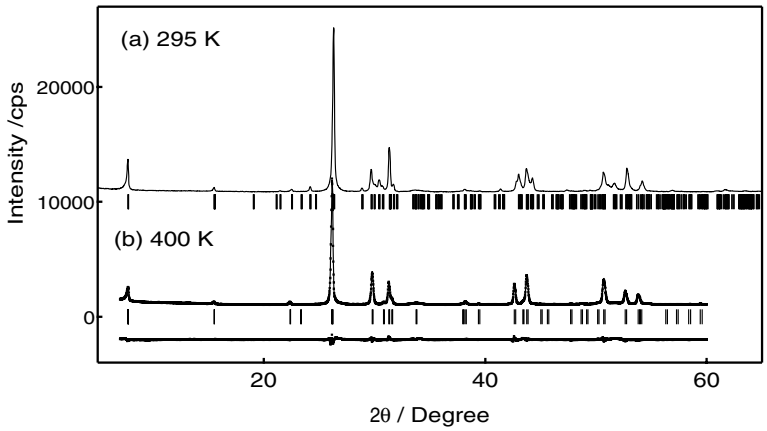

Figure 1. X-ray diffraction patterns at (a) 295 K and (b) 400 K for $PbSnF_4$.

Table 1. Crystallographic data of $PbSnF_4$ at 295 and 400 K.

	295 K	400 K
Space group	$Pna2_1$ (No 33)	$I4/nmm$ (No 149)
Crystal system	Orthorhombic	Tetragonal
Lattice parameters	$a = 6.002(1)$	$a = 4.2403(2)$[a]
(Å)	$b = 5.872(1)$	$c = 11.4360(6)$
	$c = 22.769(3)$	
Z	8	2
D_{calc} (g cm^{-3})	6.654	6.483

[a] Reported parameters for the tetragonal phase: $a = 4.2236(2)$ Å and $c = 11.4291(7)$ Å at RT [5].

good agreement with those reported by Reau *et al* [1]. Figure 1(a) shows an x-ray diffraction pattern of $PbSnF_4$ at 295 K. This pattern is quite similar to that of the orthorhombic phase reported by Collin *et al* [3]. However, our sample showed additional small peaks and could be indexed as an orthorhombic system with a doubling unit cell along the c-axis. On heating the sample, the powder pattern changed to a simple tetragonal one as shown in figure 1(b). This powder pattern could be easily refined by a Rietveld method using structural parameters reported by Kanno *et al* [5]. Crystallographic parameters of $PbSnF_4$ are summarized in table 1. The simulation of the powder pattern for the orthorhombic phase suggested that the structural change from the tetragonal phase is minor except the symmetry break. However, reliable positional parameters of the fluoride ions could not be determined successfully at 295 K.

3.2. Bulk dc conductivity

Figure 2 shows the Cole–Cole plots of the resistivity at selected temperatures for the $PbSnF_4$ polycrystalline sample. Below room temperature a depressed semicircle was observed accompanied by a straight line on the low-frequency side, suggesting an effect of the blocking electrodes. With increasing temperature, the radius of the depressed semicircle decreases and the semicircle moves to the high-frequency side, leaving only the capacitive blocking spike observable over the frequency range used (figure 2). This indicates that the electrode effect becomes more dominant at high temperatures, due to the high ionic conductivity of the sample.

Normally the impedance spectrum of a polycrystalline material is expected to have two semicircular arcs, one attributed to the grain and the other, low-frequency, one to the grain

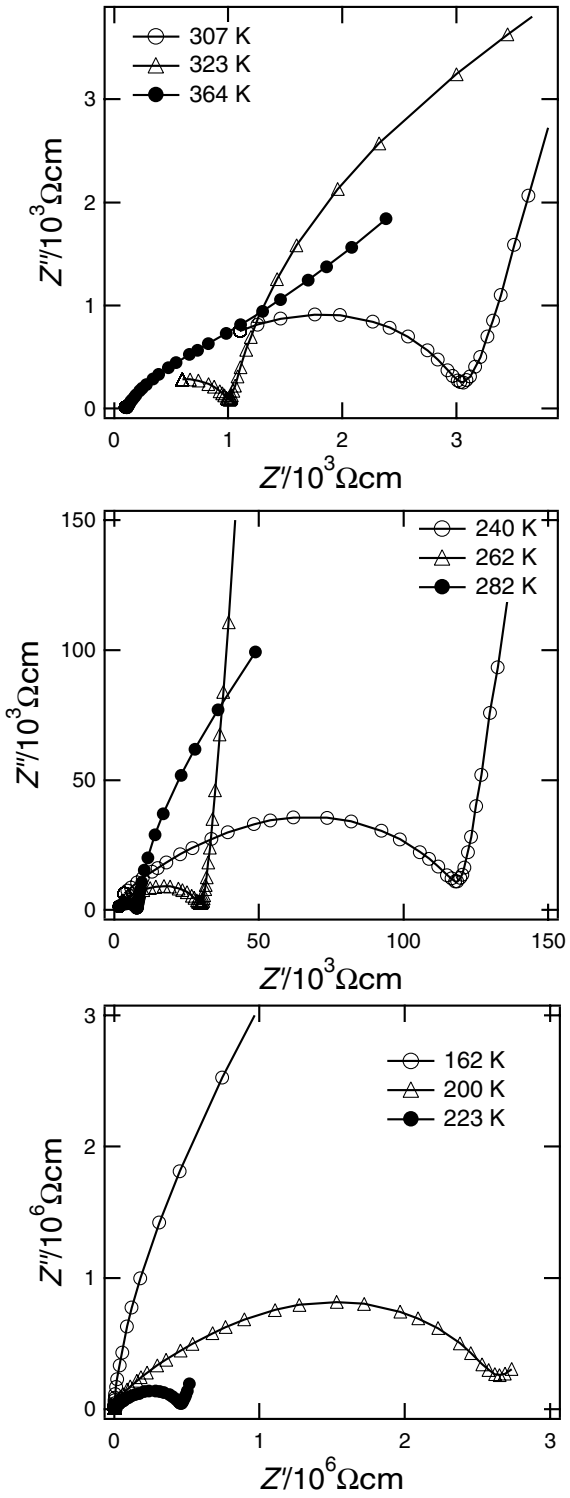

Figure 2. Cole–Cole plots of the resistivity at selected temperatures for $PbSnF_4$.

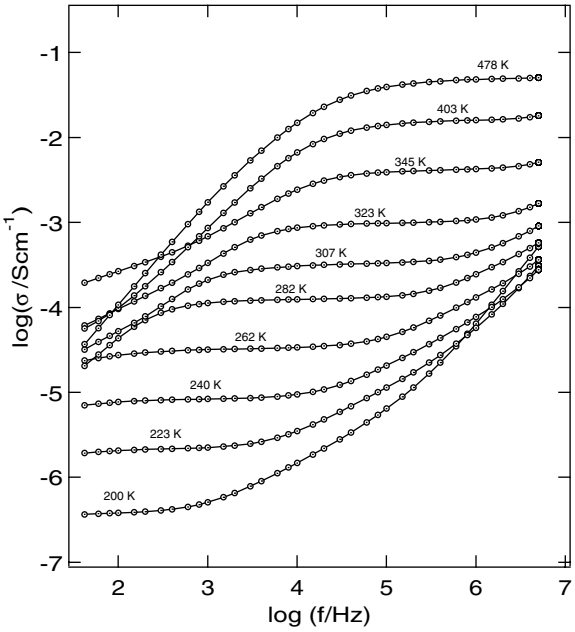

Figure 3. Frequency dependence of the real part of the conductivity Re (σ^*) at various temperatures.

boundary. However, our sample showed only one depressed (non-ideal) semicircle as shown in figure 2, whose centre is displaced below the real axis. Such non-ideal behaviour may originate from [9]

(i) the presence of a distribution in relaxation times within the bulk response or
(ii) a distortion due to other relaxations, e.g. grain boundary relaxation.

Our experimental results, however, suggest that the depressed semicircle in the impedance spectra corresponds to the bulk behaviour of the sample, as will be explained below, and there is no grain boundary contribution to the impedance spectra.

In order to check the presence of the grain boundary effect, the capacitance value was calculated at the maximum frequency, f_{max}, at the Z'' peak using a relation of $2\pi f_{max} RC = 1$. The capacitance value was of the order of $\sim$100 pF. This low capacitance value (pF order) is usually assigned to grain response rather than the grain boundary, whose higher capacitance value is in the nF–μF order [10]. The dc conductivity values extracted from the plateau region of figure 3 coincide with the bulk dc conductivity, σ_{dc}, estimated from the Cole–Cole plots (figure 2). Accordingly, the effect of the grain boundary on the impedance spectra of $PbSnF_4$ sample is excluded and the bulk resistivity of the $PbSnF_4$ sample is determined from the intersection of the semicircular arc at low frequency with the real axis.

The bulk dc conductivity (σ_{dc}) determined by the Cole–Cole plots is plotted against inverse temperature in figure 4. This temperature dependence was analysed using an Arrhenius equation,

$$\sigma T = \sigma_0 \exp(-E_\sigma / kT), \tag{2}$$

where σ_0 is the pre-exponential factor and E_σ is the activation energy for the ion migration. As figure 4 shows, the σ_{dc} versus $1/T$ curve shows two straight-line regions; i.e., a gradual change

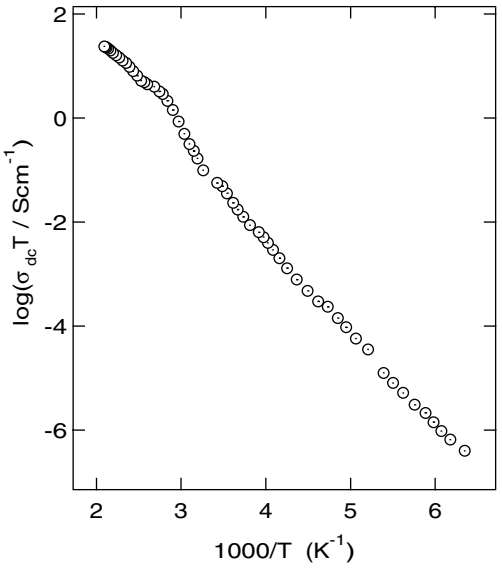

Figure 4. Bulk dc conductivity for $PbSnF_4$ as a function of the inverse temperature.

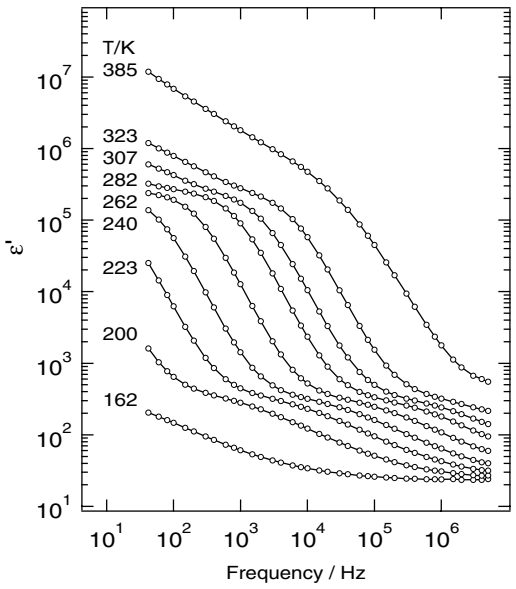

Figure 5. Frequency dependence of the dielectric constant ε' for $PbSnF_4$ at various temperatures.

of the slope was observed around 355 K in the heating process. The activation energies of conduction below and above the transition region were found to be 30(1) and 22(1) kJ mol^{-1}, respectively. Similar behaviour was observed in the cooling process with the change of the slope occurring around 340 K, which was lower than that in the heating process. The present results are inconsistent with those reported by Denes *et al* [6]. They reported that the conductivity curve contains only one straight line with activation energy of $\sim$30 kJ mol^{-1} upon cooling from 200 to 25 °C.

3.3. Frequency dependence of the conductivity

Figure 3 plots the real part of conductivity $\mathrm{Re}(\sigma^*)$ against frequency over a wide range of temperatures. The real part of the conductivity changes drastically with temperature and frequency. These conductivity versus frequency curves can be divided into three distinct regions. The first one is the low-frequency dispersion region observed above 260 K, at which the conductivity decreases with decreasing frequency. This behaviour is typical for a highly ionic conductor and can be ascribed to the space charge polarization at the blocking electrodes [11]. As the frequency decreases, more and more charge accumulation occurs at the interface between electrode and electrolyte, which leads to a drop in the conductivity at low frequencies. The second region is the frequency-independent plateau region, which appears in the intermediate-frequency region and corresponds to the bulk dc conductivity, σ_{dc}. It is interesting to note that the plateau region shifts from a low-frequency region at low temperature to a high-frequency region at high temperature. The third one appears in a lower-temperature region, at which the conductivity increases with frequency. This behaviour of the ac conductivity has been known as a universal dynamic response [12, 13], in which the ac conductivity, σ_{ac}, was found to obey the following power law:

$$\sigma_{ac}(\omega) = \sigma_{dc} + A\omega^s, \tag{3}$$

where σ_{dc} is the dc conductivity, A is a constant and s is the power-law exponent. In most cases, s is found to be between 0.6 and 1 for ionic conducting materials [14]. The value of $s = 1$ is regarded theoretically as the limiting value. The experimental values of the exponent s obtained for $PbSnF_4$ sample decrease with increasing temperature from 1.1 to 0.3. The case of $s > 1$ has been reported in a few samples of semiconductors and glasses at relatively low temperatures [15].

3.4. Dielectric studies

Complex permittivity, $\varepsilon^* = \varepsilon' - \mathrm{j}\varepsilon''$, for $PbSnF_4$ was calculated from the impedance by equation (1). Figure 5 shows a representative frequency dependence of the real part of the complex dielectric permittivity ε' as a function of temperature. The frequency dependence of the dielectric permittivity ε' shows interesting characteristic features. Two levelled-off regions appeared in the intermediate-temperature range as a function of frequency. The first levelled-off region, having a huge ε' value, is a typical consequence of the formation of the space charges near the electrodes. The second levelled-off region corresponds to the bulk conductivity and finally ε' is expected to decrease to ε_∞ at higher frequency. The huge dielectric constant of this material at low frequency suggests a possible application as an energy storage device. It is interesting to note that ε' increases further above 323 K, probably due to the phase transition to the highly conducting phase.

Figures 6(a) and (b) show the temperature dependence of the real part of the dielectric permittivity at low and high frequencies, respectively. As figure 6 shows, an anomalous dielectric peak was observed around the transition temperature of $PbSnF_4$. It can be noticed that the peak intensity decreases sharply with further increasing frequency and the peak almost disappears at higher frequencies (MHz). In addition, the dielectric peak temperature is found to be frequency independent, which indicates that there is no grain boundary or interface effect on the temperature dependence of the dielectric permittivity.

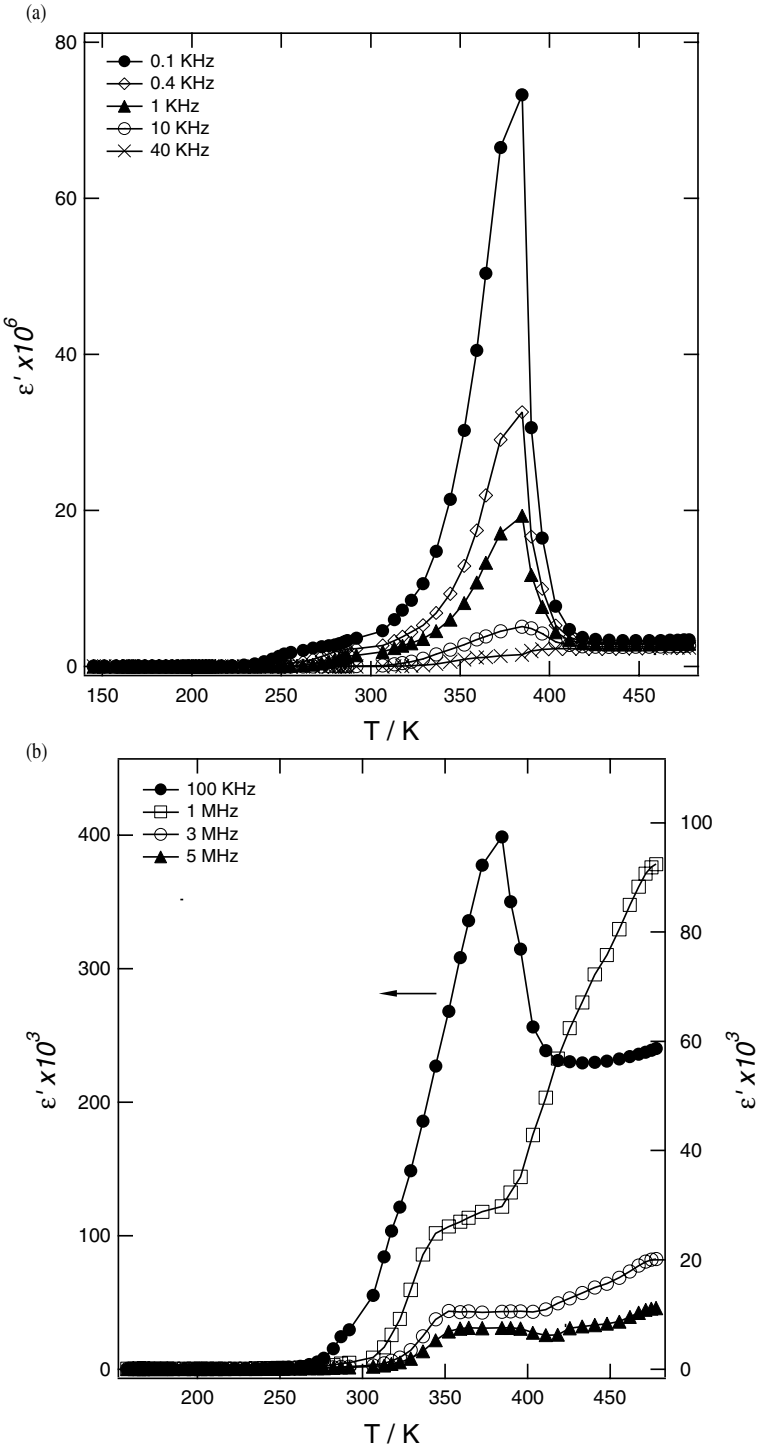

Figure 6. Temperature dependence of the dielectric constant ε' for $PbSnF_4$ at (a) low and (b) high frequencies.

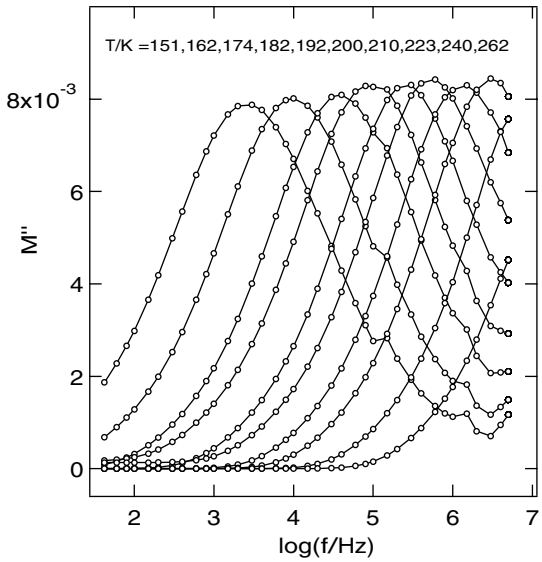

Figure 7. Imaginary part of the modulus Im (M^*) at various temperatures.

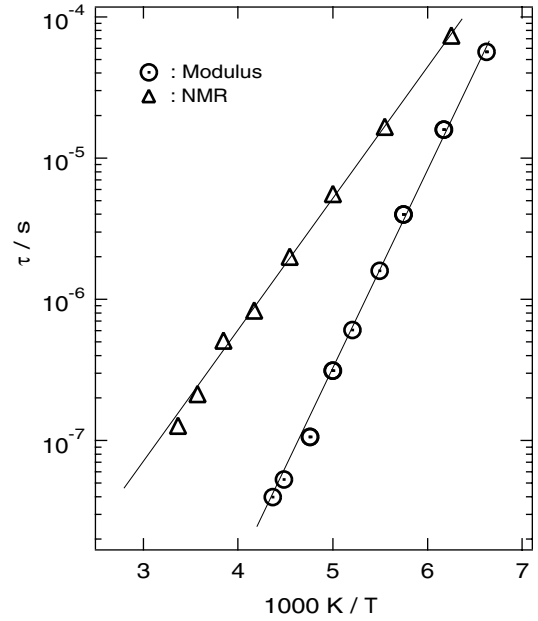

Figure 8. Arrhenius plots of the motional correlation times from the modulus and ^{19}F NMR measurements.

3.5. Conductivity relaxation time from modulus

In order to investigate the conductivity relaxation process, the modulus formalism defined by the following equation was used.

$$M^* = M' + \mathrm{j}M'' = \mathrm{j}\omega C_0 Z^*. \tag{4}$$

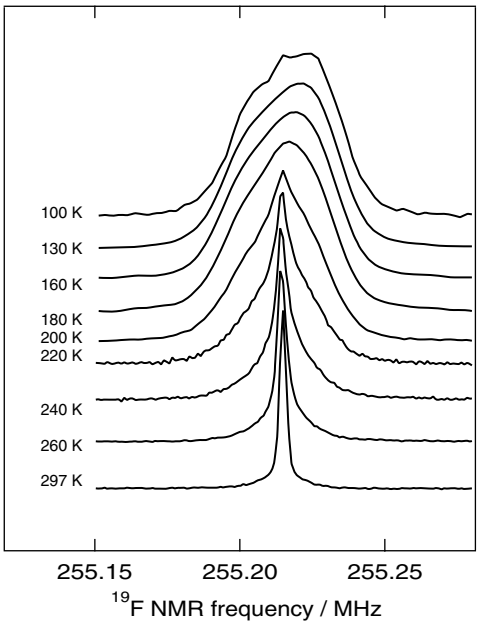

Figure 9. ^{19}F NMR spectra of $PbSnF_4$ at various temperatures.

The electric modulus representation has been widely used in analysis of the electrical properties of ionic conductors, because it gives a conductivity relaxation time for the bulk material and the effect of blocking electrodes is usually suppressed [16]. Figure 7 shows the frequency dependence of the imaginary part, M'', of the electric modulus for $PbSnF_4$ at several temperatures. Well defined peaks are observed and the peak position shifts toward higher frequency with increasing temperature. Above 240 K only a part of the peak was observed in our experiment. From the frequencies of the peak maximum (f_{max}) in M'', so-called conductivity relaxation times τ_M were determined by the relation $2\pi f_{max}\tau_M = 1$. Figure 8 plots τ_M against inverse temperature together with the motional correlation times from the ^{19}F NMR measurement. The conductivity relaxation times could be well described by the following Arrhenius expression:

$$\tau_M/s = 2.9 \times 10^{-14} \exp(27(1)\ \text{kJ mol}^{-1}/kT). \tag{5}$$

This activation energy, $E_M = 27(1)$ kJ mol^{-1}, from the modulus formalism is in good agreement with that from the dc conductivity ($E_\sigma = 30$ kJ mol^{-1}) in the same temperature range. This indicates that the movement of the fluoride ions is responsible for both the ionic conduction and the relaxation processes. However, the half-width of the modulus peak is about 2.25 decades and is considerably broad compared with the 1.14 decades which is predicted for a system with a single relaxation time. This fact suggests the highly disordered structure of this material.

3.6. ^{19}F NMR of $PbSnF_4$

Figure 9 shows ^{19}F NMR spectra observed below room temperature. The broad NMR spectra at low temperatures become narrower above 190 K. The narrowing phenomenon was observed in two steps, as shown in figure 10. The first narrowing begins at as low a temperature as 190 K and finishes at about 300 K. The narrowing limit of about 2.8 kHz confirms that all fluoride

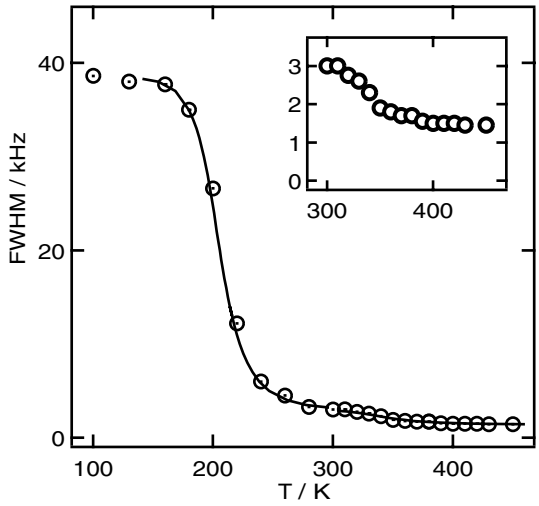

Figure 10. Temperature dependence of the line width of ^{19}F NMR spectra for $PbSnF_4$.

ions contribute to the ionic transport properties of $PbSnF_4$. The second narrowing begins at 300 K and finishes at about 400 K (the inset of figure 10), at which the phase transition to the tetragonal phase is completed. These narrowing phenomena show two different hopping mechanisms, as reported by Villeneuve *et al* [17]. In order to estimate the correlation time (τ_{NMR}) for the anionic diffusion, the line width at the first narrowing region was analysed by the following equation [18]:

$$\tau_{NMR} = \tan[\pi(\Delta H^2 - A^2)/2(B^2 - A^2)]/2\pi\alpha\Delta H, \tag{6}$$

where A, ΔH and B represent the line widths at temperatures above, within and below the transition region, respectively, and α is a constant near unity. A and B were estimated from the graph to be 2.8 and 38.4 kHz, respectively. τ_{NMR} are plotted in figure 8 and are compared with τ_M. The activation energy determined from the temperature dependence of τ_{NMR} was found to be 18.5 kJ mol^{-1}. This activation energy value is much smaller than the activation energy for the dc conductivity, suggesting that not only translational diffusion but also some local motion of the fluoride ions contributes to the narrowing.

4. Conclusions

The phase transition of superionic $PbSnF_4$ was detected by DTA ($T_{tr} = 340$ K). X-ray diffraction followed by Rietveld analysis suggests an orthorhombic to tetragonal phase transition. Moreover, a change of the slope in the σ_{dc} versus $1/T$ plot was observed around 355 K. The activation energy of the conductivity decreased from 30 to 22 kJ mol^{-1} at the phase transition. This phase transition was also detected by the dielectric anomaly measured at several frequencies.

A low-frequency dispersion of the ac conductivity was observed due to the accumulation of charge carriers at the electrode–electrolyte interface, and this phenomenon became more dominant at high temperatures. Associated with this interfacial effect a huge dielectric constant was observed at low frequency. The electric modulus peak was observed at low temperature due to the conductivity relaxation process, and the activation energy deduced from the τ_M versus $1/T$ plot agreed well with that from σ_{dc}. Although ^{19}F NMR supported the high conductivity

due to the motion of fluoride ions, the activation energy calculated from the NMR correlation times was smaller than that from the conductivity measurements, suggesting the existence of local motion.

References

[1] Reau J-M, Lucat C, Portier J, Hagenmuller P, Cot L and Vilminot S 1978 *MRS Bull.* **13** 877
[2] Donaldson J D and Senior B J 1967 *J. Chem. Soc.* A 1821
[3] Collin A, Denes G, Le Roux D, Madamba M C, Parris J M and Salaun A 1999 *Int. J. Inorg. Mater.* **1** 289
[4] Chadwick A V, Hammann E-S, van der Putten D and Strange J H 1987 *Cryst. Lattice Defects Amorphous Mater.* **15** 303
[5] Kanno R, Nakamura S, Ohno K and Kawamoto Y 1991 *MRS Bull.* **26** 1111
[6] Denes G, Milova G, Madamba M C and Perfiliev M 1996 *Solid State Ion.* **86–88** 77
[7] Wakagi A, Kuwano J, Kato M and Hanamoto H 1994 *Solid State Ion.* **70/71** 601
[8] Wakagi A and Kuwano J 1994 *J. Mater. Chem.* **41** 973
[9] El Omari M, Senegas G and Reau J-M 1998 *Solid State Ion.* **107** 281
[10] Hodge I M, Ingram M D and West A R 1976 *J. Electroanal. Chem.* **74** 125
[11] MacDonald J R 1987 *Impedance Spectroscopy* (New York: Wiley)
[12] Jonscher A K 1977 *Nature* **267** 673
[13] Funke K 1993 *Prog. Solid State Chem.* **22** 111
[14] Lee W K, Liu J F and Nowick A S 1994 *Phys. Rev. Lett.* **67** 1559
[15] Elliot S R 1987 *Adv. Phys.* **36** 135
[16] Ambrus J H, Moynihan C T and Macedo P B 1972 *J. Phys. Chem.* **76** 3287
[17] Villeneuve G, Echegut P, Lucat C, Reau J-M and Hagenmuller P 1980 *Phys. Status Solidi* b **97** 295
[18] Abragam A 1961 *Principles of Nuclear Magnetism* (London: Oxford University Press) ch 5